Field-aligned magnetohydrodynamic bow shock flows in the switch-on regime

Parameter study of the flow around a cylinder and results for the axi-symmetrical flow over a sphere

H. De Sterck[*] **and S. Poedts**[**]

Center for Plasma Astrophysics, Katholieke Universiteit Leuven, Celestijnenlaan 200B, B-3001 Heverlee, Belgium
(hans.desterck@wis.kuleuven.ac.be; stefaan.poedts@wis.kuleuven.ac.be)

Abstract. A parameter study is undertaken for steady symmetrical planar field-aligned MHD bow shock flows around a perfectly conducting cylinder. For sets of values of the inflow plasma β and Alfvénic Mach number (M_A) which allow for switch-on shocks, a numerical solution is obtained which exhibits a complex bow shock shape and topology with multiple shock fronts and a dimpled leading front. For parameter values outside the switch-on domain, a classical single-front bow shock flow is obtained. These results show that the β and M_A parameter regime for which the complex bow shock topology occurs, corresponds closely to the parameter regime for which switch-on shocks are possible.

The axi-symmetrical field-aligned bow shock flow over a perfectly conducting sphere is then calculated for one set of values for β and M_A in the switch-on domain, resulting in a complex bow shock topology similar to the topology of the flow around a cylinder.

These complex shock shapes and topologies may be encountered in low-β space plasmas. Fast coronal mass ejections moving away from the sun in the low-β inner corona may induce preceding shock fronts with upstream parameters in the switch-on domain. Planetary and cometary bow shocks may have upstream parameters in the switch-on domain when the impinging solar wind occasionally becomes low-β. The simulation results may be important for phenomena in the Earth's magnetosheath.

Key words: Magnetohydrodynamics (MHD) – shock waves – methods: numerical – Sun: corona – comets: general – planets and satellites: general

1. Introduction

Shock phenomena are abundant in space physics plasmas. Large-scale flows involving shocks are often modeled as 'continuous fluids' and described by the equations of hydrodynamics and magnetohydrodynamics (MHD) (e.g. Petrinec & Russell 1997). Bow shocks are formed when the solar wind encounters comets (e.g. Gombosi et al. 1994, 1996) and planets (e.g. Wu 1992, Tanaka 1993, Song & Russell 1997). Shocks play an important role in the magnetic topology of the heliosphere which interacts with the interstellar wind (e.g. Pogorelov 1995, Pogorelov & Semenov 1997, Linde et al. 1998, Ratkiewicz et al. 1998). Helios 1 spacecraft observations have detected interplanetary shocks which are well correlated with fast solar coronal mass ejections (CMEs) observed by the Solwind coronagraph (Sheeley et al. 1985), and some bright features present in SMM coronagraph images have been interpreted as signatures of shocks induced by fast CMEs (Steinolfson & Hundhausen 1990a, 1990c, Hundhausen 1998).

Hydrodynamic bow shocks around a cylindrical object have the classical form and topology of Fig. 1a, with a single shock front which is concave-inward (to the object). Most MHD bow shocks described in the space physics literature have the same simple shape and topology, but recent numerical simulation results have revealed a MHD bow shock flow which exhibits a more complex shape and topology, for the case of a low inflow plasma β and an inflow Alfvénic Mach number M_A which corresponds to moderately super-Alfvénic flow. De Sterck et al. (1998b) study the steady state planar ($B_z \equiv 0$ and $v_z \equiv 0$) field-aligned bow shock flow with top–bottom symmetry around a perfectly conducting cylinder for one set of parameters in this parameter domain. They describe a steady state bow shock flow which exhibits a complex multiple-front shape and topology. The bow shock solution is shown in Fig. 2, and the topology of the flow is sketched in Fig. 1b. The leading shock front contains a concave-outward 'dimple', and is followed by several other discontinuities. The 'dimpling' of shock fronts in a low-β plasma had been observed earlier in time-dependent numerical simulations of CMEs moving faster than the Alfvén speed, and dimpled
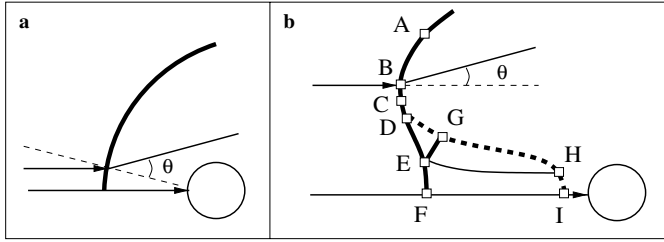
Fig. 1a and b. Possible bow shock topologies for a 2D uniform flow (streamlines have arrows) falling in on a cylinder from the left. Shock normals are shown as thin dashed lines. **a** Traditional single-front bow shock topology. **b** Complex multiple-front bow shock topology which appears for the field-aligned MHD bow shock flow of Fig. 2 with parameters in the switch-on domain.
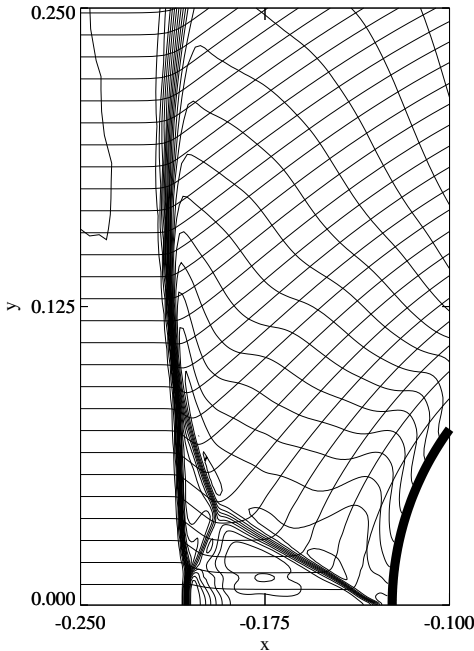

Fig. 2. Part of the steady bow shock solution for one set of inflow parameters in the switch-on domain obtained in De Sterck et al. (1998b) (inflow Mach number $M_A = 1.5$ and inflow plasma $\beta = 0.4$, 120×120 grid). We show density contours (piling up in the shocks) and magnetic field lines (coming in horizontally on the left). The flow comes in from the left. The cylinder is situated on the right (thick solid). The leading shock front is slightly dimpled. In the central part of the flow, a second front has separated and is trailing the leading front. Additional discontinuities can be seen in the central interaction region. The topology of the flow is sketched in Fig. 1b. The shocks are fast, hydrodynamic, and intermediate, as discussed in Sect. 2.1.

bright features in coronagraph images have been related to dimpled shock fronts preceding super-Alfvénic CMEs (Steinolfson & Hundhausen 1990a, 1990c, Hundhausen 1998). These effects have to be clearly separated from the observed concave-outward shapes of some *slow* (sub-Alfvénic) CME fronts, which have been related to the geometrical properties of *slow* MHD shocks (Steinolfson & Hundhausen 1990b). In this paper we discuss the geometrical shapes of *fast* (super-Alfvénic) MHD bow shocks.

Theoretical reasoning based on symmetry considerations has proposed the possible occurrence of fast switch-on shocks in a parameter regime which is called the switch-on regime, as an explanation for the occurrence of multiple-front MHD bow shocks and the dimpling of the leading shock front of fast CMEs (Steinolfson & Hundhausen 1990a, 1990c, Hundhausen 1998, De Sterck et al. 1998b). This line of thought will be clarified in Sect. 2.1. This reasoning predicts complex bow shock topologies for all bow shock flows with parameters in the switch-on regime. In the present paper we will verify this prediction.

In the present paper we extend the numerical results of De Sterck et al. (1998b) on MHD bow shock topology in the switch-on regime in two ways. In Sect. 3 we carry out a detailed parameter study of symmetrical planar ($B_z \equiv 0$ and $v_z \equiv 0$) field-aligned bow shock flows around a cylinder. We study how the shape and topology of the bow shock solution which was obtained by De Sterck et al. (1998b) for one particular set of parameters within the switch-on domain, changes when parameters are varied within the switch-on domain and when parameters are taken outside the switch-on domain. In Sect. 4 we present results for the axi-symmetrical field-aligned bow shock flow over a perfectly conducting sphere for a set of parameters in the switch-on domain. The presentation of these results is preceded by a short discussion in Sect. 2 of the properties of MHD shocks and the switch-on regime, and a discussion of the numerical solution technique. Finally, our conclusions are formulated and discussed in Sect. 5.

These extended results on MHD bow shock flows in the switch-on regime, together with the detailed discussion of one example of a complex bow shock flow in De Sterck et al. (1998b), form an extension of the general theory and phenomenology of MHD bow shock flows, with possible applications in space physics (Petrinec & Russell 1997).

2. Properties of MHD shocks and numerical solution of the MHD equations

2.1. Properties of MHD shocks

The complex topology of bow shock flows in the switch-on regime can be understood in terms of the properties of MHD shocks. This will be explained in the present section. Contrary to the hydrodynamic equations, which allow for only one wave mode, the MHD equations allow for three distinct wave modes, the fast magneto-acoustic wave, the Alfvén wave, and the slow magneto-acoustic wave, with (positive) anisotropic wave speeds satisfying $c_f \geq c_A \geq c_s$ in standard notation. Three types of shocks are described by the MHD equations, connecting plasma states which are traditionally labeled from 1 to 4, with state 1 a super-fast state, state 2 sub-fast but super-Alfvénic, state 3 sub-Alfvénic but super-slow, and state 4 sub-slow (Landau & Lifshitz 1984, Anderson 1963, De Sterck et al. 1998b). Fast 1–2 MHD shocks refract the magnetic field away from the shock normal. Intermediate MHD shocks (1–3, 1–4, 2–3, and 2–4) change the sign of the component of the magnetic field which is tangential to the shock front, and thus flip magnetic field lines over the shock normal. A special case of a 1–4 intermediate

shock is a 1–4 hydrodynamic (intermediate) shock, for which the magnetic field is perpendicular to the shock and does not change through the shock. Slow 3–4 MHD shocks refract the magnetic field towards the shock normal.

In De Sterck et al. (1998b) the types of the discontinuities that are present in the complex bow shock flow of Fig. 2 are clearly identified. The results of this detailed analysis can be summarized as follows, using the lettering labels of Fig. 1b. Shock parts A–B and D–E are 1–2 fast shocks, E–F is a 1–4 hydrodynamic shock, and B–C–D is a 1–3 intermediate shock. E–G is a 1=2–3=4 intermediate shock. D–G–H–I is a 2–4 intermediate shock. E–H is a tangential discontinuity. Other tangential discontinuities stretch out from points G and H along the streamlines to infinity. The reader can verify in Fig. 2 that all the intermediate shocks indeed flip magnetic field lines over the shock normal.

We remark here that the presence of intermediate shocks in this flow is an important illustration in two dimensions (2D) of many of the new theoretical results on the existence of intermediate shocks (Wu 1991, Freistuehler & Szmolyan 1995, Myong & Roe 1997). We refer to De Sterck et al. (1998b) for a discussion of this subject. Analysis of this stationary flow in terms of steady state characteristic curves and elliptic and hyperbolic regions, shows that this flow contains a steady state analog of an xt MHD compound shock (Brio & Wu 1988, Myong & Roe 1997), which is a manifestation of the non-convex nature of the MHD equations (De Sterck, Low, & Poedts, submitted to *Phys. Plasmas*). It is important to note that there is still discussion about the stability of intermediate shocks against non-planar perturbations (Wu 1991, Barmin et al. 1996), and it will be interesting to see how the intermediate shocks present in our 2D planar simulation results, would survive in a three-dimensional (3D) context which allows for non-planar perturbations. This remains subject of further work.

A fast switch-on shock is a limiting case of the fast shock for which the upstream magnetic field direction coincides with the direction of the shock normal, and the downstream magnetic field makes a finite angle θ with the shock normal. The downstream normal plasma speed exactly equals the downstream normal Alfvén speed in the shock frame. The component of the magnetic field parallel to the shock surface is thus effectively 'switched on' in going from the upstream to the downstream state of the shock. The shock at point B in Fig. 1b is an example of a fast switch-on shock. From the MHD Rankine-Hugoniot relations one can derive (Kennel et al. 1989) that switch-on shocks can be encountered for upstream parameters satisfying

$$\beta < 2/\gamma, \tag{1}$$

and

$$1 < M_A < \sqrt{\frac{\gamma(1-\beta)+1}{\gamma-1}}, \tag{2}$$

with $\beta = 2p/B^2$ the plasma β, and the Alfvénic Mach number given by $M_A = v/c_A$, where v is the plasma velocity and c_A the Alfvén speed along the shock normal. For $\gamma = 5/3$, the
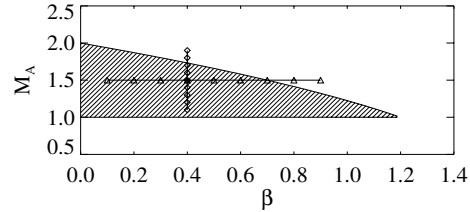

Fig. 3. Parameter domain for which switch-on shocks are possible. For $\gamma = 5/3$, switch-on shocks are possible for upstream values of β and M_A located in the shaded region. In Sect. 3, numerically obtained bow shock flows are presented for inflow quantities with fixed $\beta = 0.4$ and M_A varying from 1.1 to 1.9 (the diamonds on the vertical line), and with fixed $M_A = 1.5$ and β varying from 0.1 to 0.9 (the triangles on the horizontal line).

parameter domain in the $\beta - M_A$ plane for which switch-on shocks can occur, is sketched in Fig. 3.

These properties of MHD shocks allow us to understand why the classical single shock front solution of Fig. 1a is not found for MHD bow shocks in the switch-on regime. Because of symmetry, the magnetic field line which coincides with the stagnation streamline (stretching horizontally from infinity to the stagnation point ($v = 0$) at the cylinder) has to be a straight line. In other words, on this line, the field is not deflected by the shock. Away from this line along the shock front, the shock has to be a fast MHD shock, with the field refracted away from the normal (Fig. 1a) in order to have the post-shock flowing plasma drape around the cylinder. As we move along this fast shock front closer and closer to the intersection of the front with the stagnation line, the upstream tangential component of the magnetic field goes to zero. But when the upstream parameters lie in the switch-on domain, the downstream tangential component of the magnetic field does not vanish as we approach this intersection point, resulting in a switch-on shock with a finite turning angle θ, as illustrated in Fig. 1a. Clearly, approaching the stagnation line from its two sides along the fast shock front, would lead to two switch-on shocks of opposite deflection. This means that there is a discontinuity between the two physical states on the two sides of the stagnation field line. Such a discontinuity is not physically justified, so the concave-inward shock geometry (as in Fig. 1a) needs to be modified in order to avoid this discontinuity. In the present paper it is studied how nature accomplishes this, i.e. what alternatives to the concave-inward shock geometry the flow finds to get around the object and how this alternative depends on the parameters that characterize the flow, viz. the plasma beta β and the Alfvénic Mach number M_A.

2.2. Numerical solution of the MHD equations

In Sect. 3, we will present numerically obtained bow shock flows around a cylinder for various parameter sets inside and outside the switch-on domain, to investigate closely the correspondence between the complex bow shock topology as it was obtained in De Sterck et al. (1998b), and the parameter domain in which switch-on shocks can occur. In Sect. 4, we will investigate the axi-symmetrical bow shock flow over a sphere. In the present

section we will briefly describe the numerical solution technique used.

In our simulations a uniform field-aligned flow in planar symmetry (Sect. 3; xyz system with $\partial/\partial z = 0$, and $B_z \equiv 0$ and $v_z \equiv 0$) or axial symmetry (Sect. 4; $xr\phi$ system with $\partial/\partial\phi = 0$, and $B_\phi \equiv 0$ and $v_\phi \equiv 0$) enters from the left and encounters a perfectly conducting rigid cylinder (Sect. 3) or sphere (Sect. 4). The magnetic field is aligned with the plasma velocity in the whole domain of the resulting stationary ideal MHD flow. The stationary bow shock flow is completely determined by the inflow β and M_A in the direction of the flow speed. We take the x axis horizontal, and we can freely choose $\rho = 1$ and $B_x = 1$ (implying that the Alfvén speed along the field lines $c_A = 1$). The pressure and velocity can then be determined from β and M_A. Finally, we take $B_y = 0$ ($B_r = 0$) and $v_y = 0$ ($v_r = 0$). As the resulting stationary ideal MHD flow is scale invariant, we can freely choose the radius of the cylinder (sphere). We take $r = 0.125$ and the cylinder (sphere) is placed at the origin of the coordinate system. We simulate the flow in the upper left quadrant, on a stretched elliptic polar-like structured grid. We impose the above described uniform flow as the initial condition. We use ghost cells to specify the boundary conditions. On the left, we impose the uniform superfast incoming flow. The obstructing object is perfectly conducting. We look for a stationary flow solution with top–bottom symmetry, such that the horizontal line which extends to the center of the cylinder is the stagnation line, parallel to the incoming flow (Fig. 1). This symmetry has to be imposed in the boundary condition on the lower border of the simulation domain in order to obtain a stationary symmetrical solution. The right outflow condition is superfast, so there we extrapolate all quantities to the ghost cells. The flow evolves in time until a converged steady state bow shock solution is obtained.

We solve the equations of ideal one-fluid MHD. In 'conservative form' these equations are given by

$$\frac{\partial}{\partial t}\begin{bmatrix} \rho \\ \rho\,\boldsymbol{v} \\ \boldsymbol{B} \\ e \end{bmatrix} + \nabla \cdot \begin{bmatrix} \rho\,\boldsymbol{v} \\ \rho\,\boldsymbol{v}\boldsymbol{v} + I\,(p + \boldsymbol{B}\cdot\boldsymbol{B}\,/2) - \boldsymbol{B}\boldsymbol{B} \\ \boldsymbol{v}\boldsymbol{B} - \boldsymbol{B}\boldsymbol{v} \\ (e + p + \boldsymbol{B}\cdot\boldsymbol{B}\,/2)\,\boldsymbol{v} - (\boldsymbol{v}\cdot\boldsymbol{B})\,\boldsymbol{B} \end{bmatrix}$$
$$= -\begin{bmatrix} 0 \\ \boldsymbol{B} \\ \boldsymbol{v} \\ \boldsymbol{v}\cdot\boldsymbol{B} \end{bmatrix} \nabla \cdot \boldsymbol{B}. \quad (3)$$

This set of equations has to be supplemented with the divergence free condition $\nabla \cdot \boldsymbol{B} = 0$ as an initial condition. Here ρ and p are the plasma density and pressure respectively, $\boldsymbol{v}$ is the plasma velocity, $\boldsymbol{B}$ the magnetic field, and

$$e = \frac{p}{\gamma - 1} + \rho\,\frac{\boldsymbol{v}\cdot\boldsymbol{v}}{2} + \frac{\boldsymbol{B}\cdot\boldsymbol{B}}{2}, \quad (4)$$

is the total energy density of the plasma. I is the unity matrix. The magnetic permeability $\mu = 1$ in our units. These equations describe the conservation of mass, momentum, magnetic field, and energy.

As proposed by Powell et al. (1995), we have put a source term proportional to $\nabla \cdot \boldsymbol{B}$ in the right hand side (RHS) of Eq. 3. Discretization of this form of the equations results in a numerical scheme which conserves the $\nabla \cdot \boldsymbol{B} = 0$ constraint up to a discretization error. This approach is an attractive alternative to the use of an extra artificial $\nabla \cdot \boldsymbol{B}$ correction in every time step obtained via solution of an elliptic equation, because it consumes less computing time and because it cures the $\nabla \cdot \boldsymbol{B}$ problems in a way which is more in harmony with the hyperbolicity of the MHD system.

We solve Eq. 3 using a conservative finite volume high resolution Godunov shock capturing scheme which is second order in space and time, employing a slope-limiter approach (Leveque 1992, Gombosi et al. 1994, Tóth & Odstrcil 1996, Linde et al. 1998) with minmod-limiting on the slopes of the primitive variables. The time-integration is explicit with a two-step Runge-Kutta method. The code was previously used for MHD simulations of interacting hot filaments in a tokamak (De Sterck et al. 1998a). For our present simulations, we use the Lax-Friedrichs numerical flux function (Leveque 1992, Tóth & Odstrcil 1996, Barmin et al. 1996), which is simple and robust. Contact and tangential discontinuities are not perfectly well resolved due to the relatively high numerical dissipation for these waves, but shocks are well resolved in steady state calculations. We did not use Roe's scheme (Roe & Balsara 1996) although this scheme in theory could resolve shocks and, especially, tangential discontinuities much better. We have found several problems while trying to apply this scheme to our simulation. Roe's scheme suffers from various instabilities, like the carbuncle-instability (Quirk 1994), and as a result of these numerical instabilities, steady state solutions could not be obtained with this scheme. Using the Lax-Friedrichs scheme, we obtained convergence of more than eight orders of magnitude in the norm of the density residual. We can remark that the code sometimes generates small spurious oscillations in the upstream part of the flow, as can be seen in Fig. 2. Such oscillations seem to be hard to avoid with shock-capturing numerical schemes, but fortunately they are very small.

The bow shock flow of Fig. 2 constitutes an interesting new test case for ideal MHD codes, because it is a well-defined problem with a simple set-up but with a wealth of MHD shocks and discontinuities in the resulting flow.

3. Parameter study of the flow around a cylinder

In this section we present numerical simulation results for symmetrical bow shock flows around a cylinder, for the values of the parameters β and M_A which are indicated by the triangles and diamonds in Fig. 3.

In Fig. 4 we show global views of the bow shock solutions for a fixed $\beta = 0.4$ and M_A varying from 1.1 to 1.9. It follows from Eq. 2 that the critical Alfvénic Mach number under which switch-on shocks can exist is $M_A = 1.732$. For inflow speeds much faster than the Alfvén speed ($c_A = 1$), the bow shock has the traditional single-front topology that is also encountered in hydrodynamic bow shocks. If the inflow speed drops below
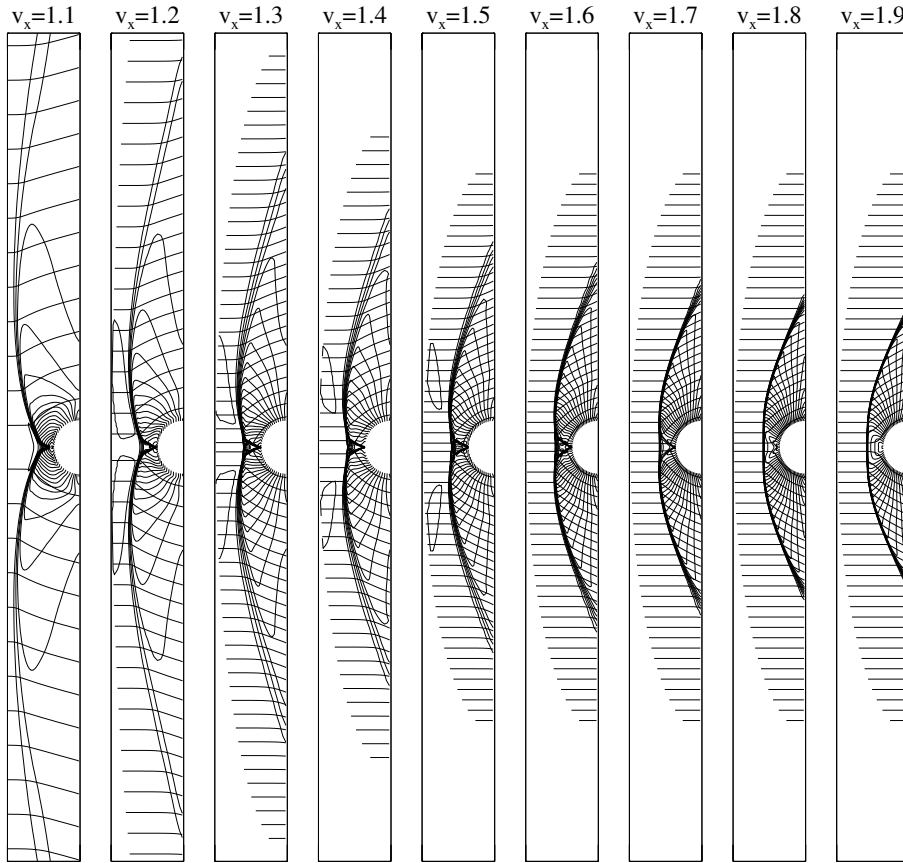
Fig. 4. Stationary bow shock solutions for fixed $\beta = 0.4$ and for varying inflow speeds (80×80 grids, $x \in [-0.35, 0]$, $y \in [-2, 2]$). Density contours pile up in shocks, and streamlines come in horizontally from the left. For inflow speeds much faster than the Alfvén speed ($c_A = 1$), the bow shock has the traditional single-front topology that is also encountered in hydrodynamic bow shocks. If the inflow speed drops below 1.732 however, a concave-outward dimple forms in the leading shock front and a second shock front appears.

1.732 however, a concave-outward dimple forms in the leading shock front and a second shock front appears. This change in shape and topology of the bow shock flow thus happens when the inflow speed becomes lower than the critical speed under which switch-on shocks are possible.

In Fig. 5 we show a detailed representation of the flow near the stagnation streamline for the bow shock solutions with varying inflow speed of Fig. 4. For inflow velocities below the critical switch-on value for the inflow speed ($M_A < 1.732$), the leading shock front has a dimpled shape. The dimpling becomes much more pronounced as the inflow velocity decreases. Below the critical inflow speed, a second shock front appears which trails the leading shock front, and additional discontinuities are present between the two shock fronts. All the shocks and discontinuities present in the topology sketch of Fig. 1b seem to be present in all the flows. Inspection of the way in which the field lines are refracted when they pass the shocks, reveals that the shocks in all the flows are of the same type as the shocks in the model flow of Fig. 2 which were discussed in Sect. 2.1, and this conclusion is confirmed by detailed analysis of upstream and downstream Mach numbers, along the lines of the detailed analysis in De Sterck et al. (1998b). For smaller inflow velocities, the central interaction region becomes smaller and the leading shocks become weaker while the trailing shock becomes stronger. As a consequence, the shock E–G of Fig. 1b can not be identified for the flow with $v_x = 1.1$ with the resolution of Fig. 5. More detailed simulations and plots (not shown)

do, however, show that shock E–G is present also for the flow with $v_x = 1.1$. For inflow velocity $v_x = 1.7$, close to the critical velocity of $v_x = 1.732$, the secondary shock fronts become weak and shock E–G can hardly be identified with the resolution of Fig. 5. For $v_x = 1.8$ the secondary (stationary) waves are still present, but they are not steepened into shocks any more. The secondary waves have disappeared almost completely for $v_x = 1.9$, and the simple single-front bow shock topology of Fig. 1a is recovered. We can thus conclude that for all the flows with parameters in the switch-on domain ($1 < M_A < 1.732$), the topology of Fig. 1b is recovered. The shapes, sizes and shock strengths of the shock parts present in the topology of Fig. 1b, vary when M_A is varied within the switch-on region. The dimple effect is more pronounced for smaller inflow Alfvénic Mach number M_A.

Above we discussed how the flow manages to go around the obstructing cylinder by adjusting the bow shock shape and topology to the inflow Alfvénic Mach number. Hereby the plasma β value was fixed to 0.4. Below we fix the inflow Alfvénic Mach number and verify how the flow modifies the geometrical structure of the bow shock when the value of the plasma β is varied.

In Fig. 6 we show global views of the bow shock solutions for a fixed $M_A = 1.5$ and β varying from 0.1 to 0.9. It follows from Eq. 2 that the critical plasma β under which switch-on shocks can exist is $\beta = 0.7$. For plasma β values larger than the critical value of $\beta = 0.7$, the bow shock has the traditional single-front
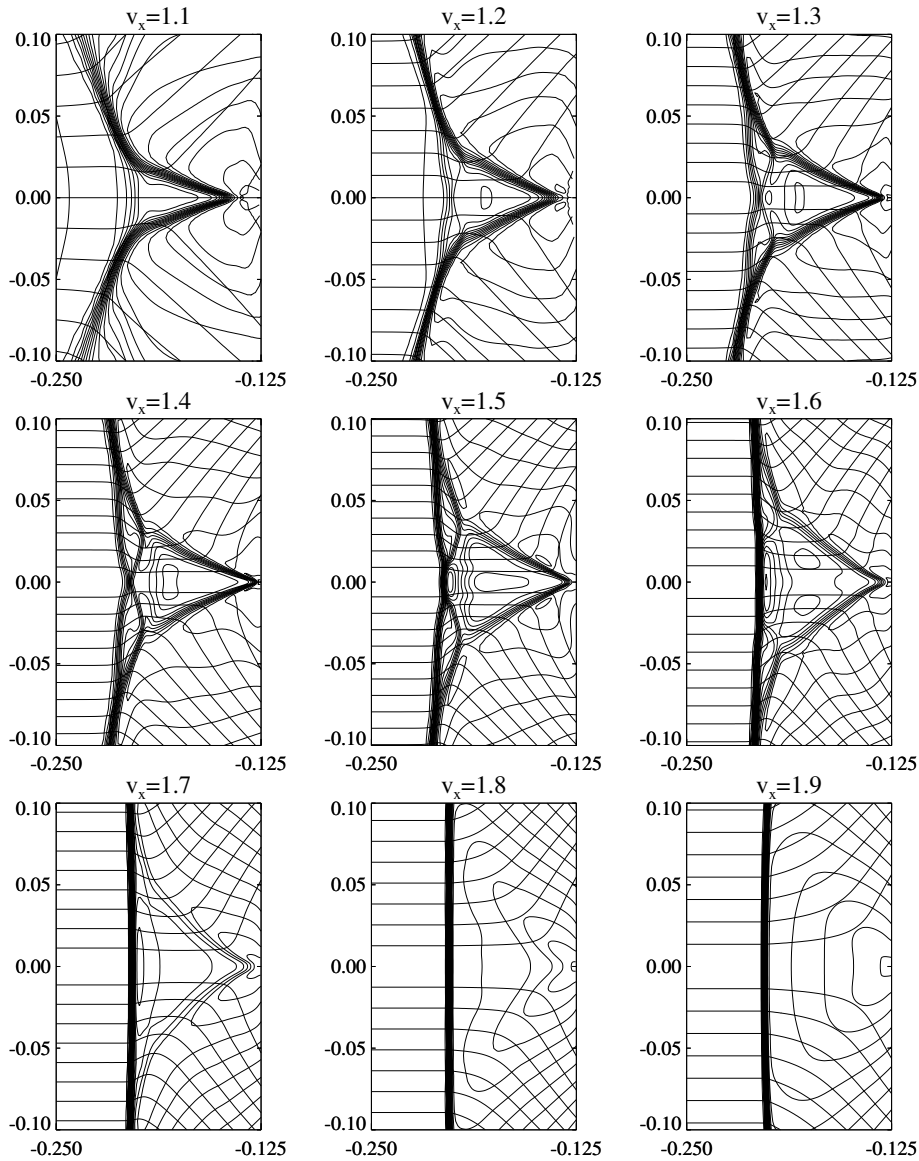
Fig. 5. Detailed representation of the flow near the stagnation streamline for the bow shock solutions with varying inflow speed and fixed $\beta = 0.4$ (80×80 grids). Density contours pile up in shocks, and streamlines come in horizontally from the left. Under the critical switch-on value for the inflow speed, the leading shock front dimples and a second shock front appears. Additional discontinuities can be seen between the two shock fronts.

topology that is also encountered in hydrodynamic bow shocks. If the plasma β drops below 0.7 however, a concave-outward dimple forms in the leading shock front and a second shock front appears. This second shock front thus appears when the plasma β becomes lower than the critical plasma β under which switch-on shocks are possible.

In Fig. 7 we show a detailed representation of the flow near the stagnation streamline for the bow shock solutions with varying plasma β of Fig. 6. For plasma β values below the critical switch-on value for the plasma β ($\beta < 0.7$), the leading shock front has a dimpled shape. The dimpling becomes more pronounced as the plasma β is decreased. Below the critical plasma β, a second shock front appears which trails the leading shock front, and additional discontinuities are present between the two shock fronts. All the shocks and discontinuities present in the topology sketch of Fig. 1b seem to be present in all the flows. Inspection of the way in which the field lines are refracted when the shocks are passed, reveals that the shocks in all the flows

are of the same type as the shocks in the model flow of Fig. 2 which were discussed in Sect. 2.1, and this conclusion is confirmed by detailed analysis of upstream and downstream Mach numbers, along the lines of the detailed analysis in De Sterck et al. (1998b). For smaller plasma β values, the central interaction region in front of the cylinder becomes smaller. As a consequence, the shock E–G of Fig. 1b can not be identified for the flow with $\beta = 0.1$ with the resolution of Fig. 7. More detailed plots (not shown) do, however, show that shock E–G is present also for the flow with $\beta = 0.1$. For plasma $\beta = 0.7$, which is the critical value, the secondary (stationary) wave has only nearly steepened into a shock. Shock E–G can not be identified for this critical value of the parameters. For $\beta = 0.8$ the secondary waves are still present, but they have not steepened into shocks any more. The secondary waves are even weaker for $\beta = 0.9$, and the simple single-front bow shock topology of Fig. 1a is recovered. We can thus conclude that for all the flows with parameter values in the switch-on domain ($\beta < 0.7$), the topology
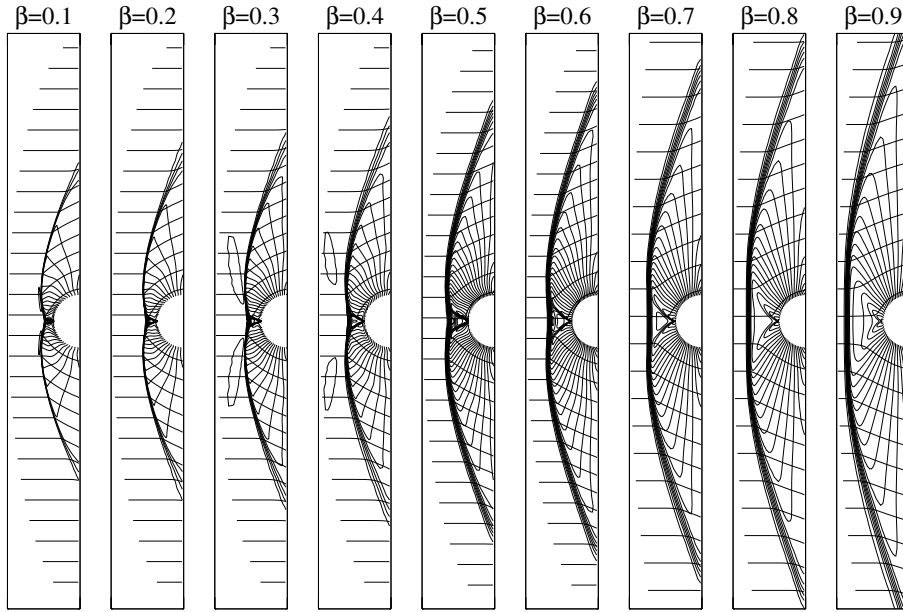
Fig. 6. Stationary bow shock solutions for fixed $M_A = 1.5$ and for varying plasma β (80×80 grids, $x \in [-0.35, 0]$, $y \in [-1.4, 1.4]$). Density contours pile up in shocks, and streamlines come in horizontally from the left. For plasma β values larger than the critical value of $\beta = 0.7$, the bow shock has the traditional single-front topology that is also encountered in hydrodynamic bow shocks. If the plasma β drops below 0.7 however, a concave-outward dimple forms in the leading shock front and a second shock front appears.
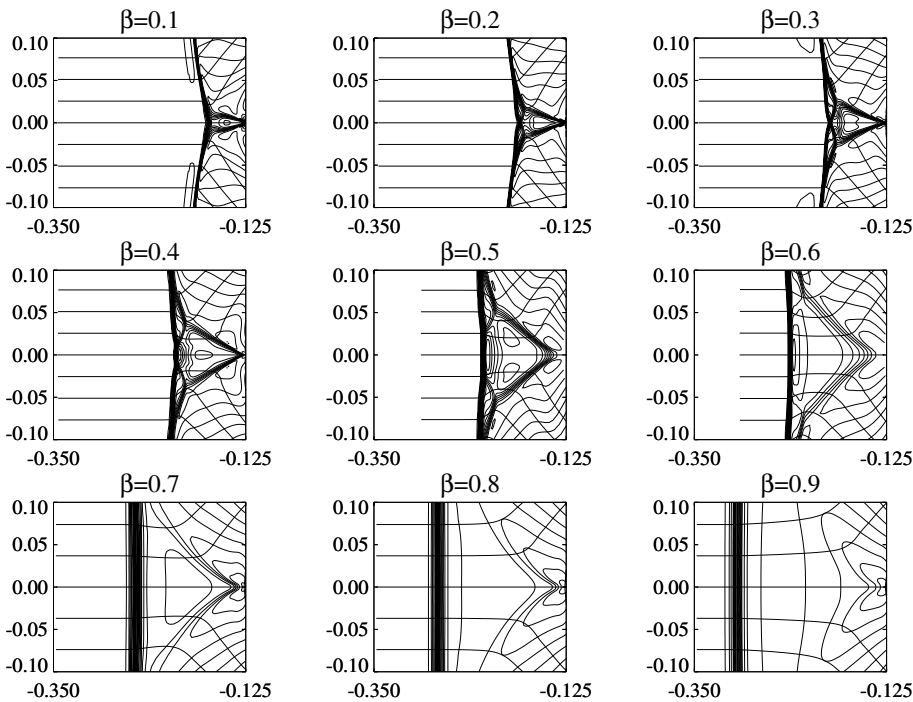

Fig. 7. Detailed representation of the flow near the stagnation streamline for the bow shock solutions with varying plasma β and for fixed $M_A = 1.5$ (80×80 grids). Density contours pile up in shocks, and streamlines come in horizontally from the left. Under the critical switch-on value for the plasma β, the leading shock front dimples and a second shock front appears. Additional discontinuities can be seen between the two shock fronts.

of Fig. 1b is recovered. The shapes, sizes and shock strengths of the shock parts present in the topology of Fig. 1b, vary when β is varied in the switch-on regime. The dimple effect is more pronounced for smaller β.

We can thus conclude from this parameter study, that there is a close correspondence between inflow parameters for which a complex bow shock topology is found, and parameters for which switch-on shocks are possible. This proves that the complex bow shock topology is indeed closely related to the possible occurrence of switch-on shocks. Because of the symmetry reasons discussed in Sect. 2.1, switch-on shocks do not occur where the leading shock fronts intersect the stagnation line. In stead, a

complex interacting shock structure with a dimpled leading front appears near that location, for the bow shock flows of Figs. 4 and 6 that have inflow parameters in the switch-on regime. Switch-on shocks are present in all these flows, however, and can be found at the locations on the leading shock fronts corresponding to point B in the topology sketch of Fig. 1b. The topology of the bow shock solution obtained in De Sterck et al. (1998b) and sketched in Fig. 1b is encountered for all the bow shock flows with parameters in the switch-on domain, and this topology is thus more generally valid than only for the single set of parameters ($\beta = 0.4$, $M_A = 1.5$) considered in De Sterck et al. (1998b). The shapes, sizes and shock strengths of the shock
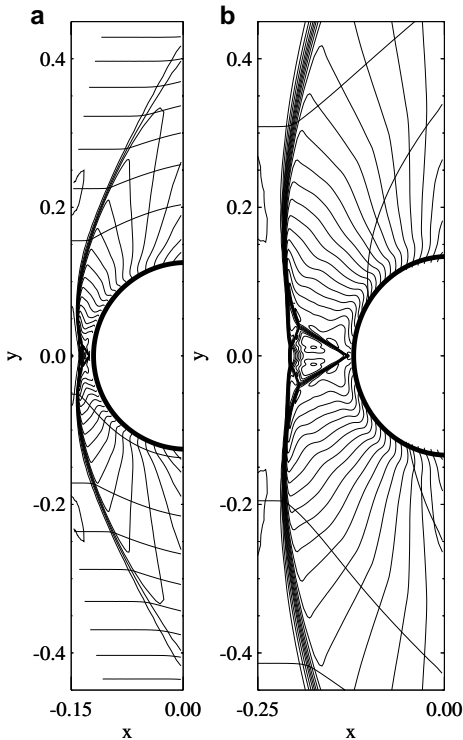
Fig. 8. **a** Steady axi-symmetrical solution of the flow over a perfectly conducting sphere, with $M_A = 1.5$ and $\beta = 0.4$ (100×100 grid). Density contours pile up in shocks, and streamlines come in horizontally from the left. **b** For comparison, the steady bow shock solution for the flow around a cylinder (Fig. 2), with the same inflow parameters. In the flow over a sphere, the shock fronts are much closer to the object than in the cylinder case, because a sphere obstructs the flow much less than a cylinder.

Fig. 9. Detail of the steady axi-symmetrical solution of the flow over a perfectly conducting sphere (100×100 grid). Density contours pile up in shocks, and streamlines come in horizontally from the left. For the symmetrical flow over a sphere, parameters in the switch-on domain lead to a complicated topology which is very similar to the topology of the flow around a cylinder.

parts present in the topology of Fig. 1b, vary when β and M_A are varied in the switch-on regime. The dimple effect is more pronounced for low values of β and M_A.

As a final remark, we can say that in the parameter regime under consideration, the global stand-off distance of the bow shocks (Petrinec & Russell 1997) decreases for increasing M_A while keeping β constant (Fig. 4) — although the stand-off distance on the stagnation line does not seem to change much (Fig. 5). The stand-off distance increases for increasing β while M_A is kept constant (Figs. 6 and 7).

4. Axi-symmetrical flow over a sphere

In this section we present numerical simulation results for an axi-symmetrical bow shock flow over a perfectly conducting sphere, for parameter values of $\beta = 0.4$ and $M_A = 1.5$ which are situated in the switch-on domain (Fig. 3). These are the same parameters as for the bow shock flow around a cylinder which was studied in De Sterck et al. (1998b). We will investigate if the axi-symmetrical bow shock flow over a sphere in the switch-on regime exhibits a complex bow shock topology similar to the topology of a flow around a cylinder in that parameter regime. In Fig. 8a we show a global view of the converged axi-symmetrical bow shock solution. The horizontal x-axis (coinciding with the
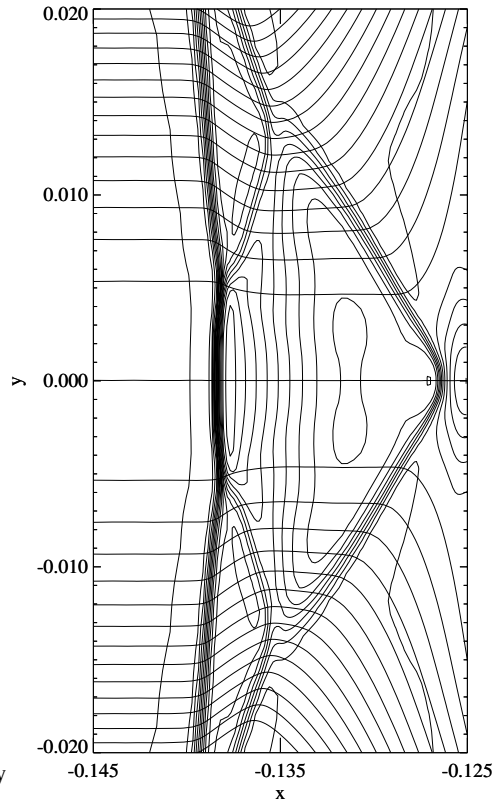
stagnation streamline) is an axis of rotational symmetry. The leading shock front shows a clear dimple, and there seem to be additional discontinuities behind the leading shock front. The shock front is much closer to the object than in the case of the flow around a cylinder with the same inflow parameters, which is shown in Fig. 8b for comparison.

In Fig. 9 we show a detailed representation of the central part of the axi-symmetrical bow shock solution near the stagnation streamline. This plot is to be compared to its cylinder flow equivalent shown in Fig. 2 (where only the upper part of the symmetrical flow is plotted). The flow clearly exhibits a topology which is very similar to the topology of the flow around a cylinder. Inspection of the way in which the field lines are refracted when the shocks are passed, reveals that the shocks in all the flows are of the same type as the shocks in the model flow of Fig. 2 which were discussed in Sect. 2.1, and detailed analysis of upstream and downstream Mach numbers, along the lines of the detailed analysis in De Sterck et al. (1998b), confirms this conclusion.

We can thus conclude that in the switch-on regime the axi-symmetrical flow over a sphere exhibits a complex bow shock topology very similar to the topology of a bow shock flow around a cylinder in that parameter regime.

5. Conclusion

In this paper we have shown how symmetrical field-aligned bow shock flows around a perfectly conducting cylinder and over a perfectly conducting sphere exhibit a complex flow topology in a parameter regime which corresponds closely to the parameter regime for which switch-on shocks are possible. This proves that the complex bow shock topology is indeed closely related to the possible occurrence of switch-on shocks. The topology of the bow shock solution obtained in De Sterck et al. (1998b) and sketched in Fig. 1b is encountered for all the cylinder bow shock flows with parameters in the switch-on domain, and this topology is thus more generally valid than only for the single set of parameters considered in De Sterck et al. (1998b). The shapes, sizes and shock strengths of the shock parts present in the topology of Fig. 1b, vary when β and M_A are varied in the switch-on regime. The dimple effect is more pronounced for low values of β and M_A.

The parameter study of the cylinder flow and the result for the axi-symmetrical flow over a sphere are extensions of the result presented in De Sterck et al. (1998b). The results on MHD bow shock flows in the switch-on regime of the present paper, together with the detailed discussion of one example of a complex bow shock flow in De Sterck et al. (1998b), form an important extension of the general theory and phenomenology of MHD bow shock flows, with possible applications in space physics (Petrinec & Russell 1997). Fast coronal mass ejections moving away from the sun in the low-β inner corona may induce preceding shock fronts with upstream parameters in the switch-on domain. The solar wind is normally high-β, but planetary and cometary bow shocks may have upstream parameters in the switch-on domain when the impinging solar wind occasionally becomes low-β (Steinolfson & Cable 1993). The effects described by our simulations may be important for phenomena in the Earth's magnetosheath (Petrinec & Russell 1997, Song & Russell 1997).

The current 2D results, however, do not complete the theory of MHD bow shocks in the switch-on regime. If we want to relax the condition on field-aligned flow by allowing for a finite angle between the incoming velocity and magnetic field, we have to consider the 3D ideal MHD problem of a stationary flow around a sphere, because in a 2D flow the magnetic flux can not be carried around a cylinder without reconnection when the flow is not field-aligned. In this case the flow will lose some of its symmetries and the stationary solution may be different. It will be interesting to see how the intermediate shocks present in our 2D planar simulation results, would survive in a 3D context which allows for non-planar perturbations. Preliminary results show that also in the 3D case the leading shock front is dimpled and is followed by a second intermediate shock front. This remains subject of further study.

References

Anderson J.E., 1963, Magnetohydrodynamic shock waves. Ph.D. Thesis, M. I. T.
Barmin A.A., Kulikovskiy A.G., Pogorelov N.V., 1996, J. Comput. Phys. 126, 77
Brio M., Wu. C.C., 1988, J. Comput. Phys. 75, 400
De Sterck H., Poedts S., Goedbloed J.P., 1998a, J. Plasma Physics 59/2, 277
De Sterck H., Low B.C., Poedts S., 1998b, Phys. Plasmas 5/11, 4015
Freistuehler H., Szmolyan P., 1995, SIAM J. Math. Anal. 26(1), 112
Gombosi T.I., Powell K.G., De Zeeuw D.L., 1994, J. Geophys. Res. 99(A11), 21525
Gombosi T.I., De Zeeuw D.L., Haberli R.L., Powell K.G., 1996, J. Geophys. Res. 101, 15233
Hundhausen A.J., 1998, Coronal mass ejections. In: Strong K.T., Saba J.L.R., Haisch B.M., Schmelz J.T. (eds.) The many faces of the sun. Springer-Verlag, New York, 143
Kennel C.F., Blandford R.D., Coppi P., 1989, J. Plasma Physics 42, 299
Leveque R.J., 1992, Numerical Methods for Conservation Laws. Lectures in Mathematics ETH Zurich, Birkhauser-Verlag, Basel
Linde T.J., Gombosi T.I., Roe P.L., Powell K.G., De Zeeuw D.L., 1998, J. Geophys. Res. 103(A2), 1889
Landau L.D., Lifshitz E. M, 1984, Electrodynamics of continuous media. Pergamon Press, Oxford
Myong R.S., Roe P.L., 1997, J. Plasma Physics 58, 521
Petrinec S.M., Russell C.T., 1997, Space Sci. Rev. 79, 757
Pogorelov N.V, 1995, A&A 297, 835
Pogorelov, N.V., Semenov A.Yu., 1997, A&A 321, 330
Powell K.G., Roe P.L., Myong R.S., Gombosi T.I., De Zeeuw D.L., 1995, AIAA Paper 95-1704-CP
Quirk J.J., 1994, Int. J. Numer. Methods Fluids 18, 555
Ratkiewicz R., Barnes A., Molvik G.A., et al., 1998, A&A 335, 363
Roe P.L., Balsara D.S., 1996, SIAM J. Appl. Math. 56, 57
Sheeley N.R. Jr., Howard R.A., Michels D.J., et al., 1985, J. Geophys. Res. 90, 163
Song P., Russell C.T., 1997, Adv. Space Res. 20, 747
Steinolfson R.S., Cable S., 1993, Geophys. Res. Lett. 20(8), 755
Steinolfson R.S., Hundhausen A.J., 1990a, J. Geophys. Res. 95(A5), 6389
Steinolfson R.S., Hundhausen A.J., 1990b, J. Geophys. Res. 95, 15251
Steinolfson R.S., Hundhausen A.J., 1990c, J. Geophys. Res. 95(A12), 20693
Tanaka T., 1993, J. Geophys. Res. 98(A10), 17251
Tóth G., Odstrcil D., 1996, J. Comput. Phys. 128, 82
Wu C.C., 1991, New theory of mhd shock waves. In: Shearer M. (ed.) Viscous profiles and numerical methods for shock waves. SIAM Proceedings Series, SIAM, Philadelphia, 209
Wu C.C., 1992, Geophys. Res. Lett. 19(2), 87